Eur. Phys. J. E **8**, 539–547 (2002)
DOI 10.1140/epje/i2002-10044-x

THE EUROPEAN PHYSICAL JOURNAL E

Networks of helix-forming polymers

S. Kutter[a] and E.M. Terentjev

Cavendish Laboratory, University of Cambridge, Madingley Road, Cambridge CB3 0HE, UK

Received 5 July 2002 /
Published online: 16 October 2002 –

Abstract. Biological molecules can form hydrogen bonds between nearby residues, leading to helical secondary structures. The associated reduction of configurational entropy leads to a temperature dependence of this effect: the *helix-coil transition*. Since the formation of helices implies a dramatic shortening of the polymer dimensions, an externally imposed end-to-end distance R affects the equilibrium helical fraction of the polymer and the resulting force-extension curves show anomalous plateau regimes. In this article, we investigate the behaviour of a crosslinked network of such helicogenic molecules, particularly focusing on the coupling of the (average) helical content present in a network to the externally imposed strain. We show that both elongation and compression can lead to an increase in helical domains under appropriate conditions.

PACS. 78.20.Ek Optical activity – 83.80.Va Elastomeric polymers – 87.15.La Mechanical properties

1 Introduction

Recent advances in experimental techniques allow to perform single-molecule experiments on polymer chains. Typical experiments, for example with an atomic-force microscope [1–4], reveal a characteristic force-extension curve of a molecule. However, theoretical understanding is often limited, if not poor, due to the complicated nature of interactions between individual parts of the molecule: the force-extension behaviour strongly depends on the microscopic configurations of the polymer, which, for complex biological molecules can exhibit a very rich energy landscape with respect to configurational coordinates. In this case, one expects a strong dependence on the actual pathways of unfolding and folding, respectively. Furthermore, the experimental manipulation might influence the dynamics of the molecule in this energy landscape such that the ordinary equilibrium statistical mechanics breaks down and the system behaves non-ergodically.

However, certain homopolypeptides form long strands of helical segments of regular α-helices under appropriate conditions (see Fig. 1), hence the folding pathways are very simple in this case: on a coarse-grained level, the internal states of these molecules are described according to the Zimm-Bragg model [5]: it assumes that each segment along the polymer backbone has access to merely two states, a random coil-like, unbound state and a helical state, where the particular residue forms a hydrogen bond with specific other residues at a certain distance along the backbone. The state of the polymer can therefore be described by a simple sequence $\{hhcchchc\dots\}$, where c and h stand for the coil or helical state of each listed segment. The interactions come into play by the use of an appropriate Hamiltonian, which can be of arbitrary sophistication, for example taking into account the fact that segments can only form a H-bond with, for instance, their fourth neighbours [7–9]. This allows to compute key properties of a molecule, *e.g.*, the average helical fraction in a chain, by applying standard methods of statistical mechanics. Experimentally, one can determine the fraction of monomers in a helical state by measuring the optical activity in a solution of helix-forming chains. Since, due to the coherent ordering, helical domains rotate the polarisation of light much more strongly than the individual chiral monomers in the coil state, the measure of optical activity gives a direct indication of the fraction of monomers in the helical state [10–12].

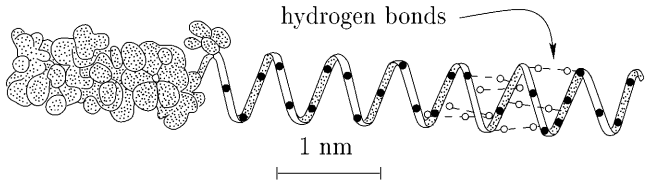

Fig. 1. An α-helix of a polymer, showing in a schematic way the van der Waals radii on the left, the backbone in the center and the hydrogen bonds between residues on the right, after [6].

This approach can be extended to deal with the case where the end-to-end distance R is constrained externally. Recently, two different groups [13–15] have independently

[a] e-mail: kutter@cantab.net

calculated the effects of such a constraint on the force and the helical fraction, revealing large plateaus in the force-extension curve and the formation of helical domains upon stretching. In contrast to the end-to-end distance, which can be controlled experimentally, the helical fraction cannot be determined for a single molecule. On the other hand, as mentioned above, the average helical fraction of solutions is perfectly accessible, whereas now the end-to-end distance of individual molecules is left uncontrolled. In order to determine the relationship between the helical fraction and the end-to-end distance, one needs to be able to control the end-to-end distance and to simultaneously measure the helical content.

We show that a network made of helix-forming polymer molecules can provide a system which fulfills both requirements: a macroscopic deformation is experimentally easy to impose and affects the end-to-end distance of network strands. At the same time, the optical activity can be monitored, provided the sample is sufficiently transparent.

However, there is a price to pay: random polymer networks are very complex and poorly understood systems: topological constraints alter the statistics due to the fact that the endpoints of strands are crosslinked to each other and different chain segments cannot intersect. The crosslinked network remembers its history: its properties depend on the conditions at the moment of its formation.

Although any network theory faces numerous difficulties, the most simple approach of the *phantom chain network* is frequently and successfully used. In this model, the chains are assumed to interact at their endpoints only, *i.e.* at the crosslinks. The model neglects the interaction along the backbone, and therefore assumes the chains to be transparent to each other and free to intersect. Despite its simplicity, the model reproduces many aspects of the experimental data [16].

In this article, we unite two approaches, the statistical mechanics of a single helix-forming molecule and a basic network theory. We base our investigations on the ideas by Buhot and Halperin [13,14] for the response of a single helix-forming molecule to an externally imposed end-to-end extension and on the phantom chain network approach to therefrom calculate the network properties.

Our approach not only provides a useful extension of the single chain theory, but also offers a way to control the helical content in the network. By deforming rubber or gel, one indirectly affects the end-to-end distances of the polymer strands. As they are stretched or compressed, the average helical fraction changes. Hence, in an optically transparent gel network, one can determine the helical fraction by measuring the optical activity (as in the case of a solution [10–12]), and moreover by imposing a macroscopic deformation one can identify the coupling between mechanical and optical responses, and thus draw conclusions about the effect of deformation on the helical fraction.

The article is organised as follows: in Section 2, we review the classical Zimm-Bragg model [5] and the solution method proposed by Buhot and Halperin [13]. In Section 3, we briefly outline the phantom chain network approach to calculate network properties on the basis of single molecule parameters. Section 4 links the approaches of Sections 2 and 3 together and provides a network theory of helix-forming molecules. Analytical and numerical results, and their discussion follow in Section 5.

2 Helix-coil transition models

Our aim is to describe a network of polymers which can fold into regular α-helices, due to the formation of regularly spaced hydrogen bonds. This section reviews the principles of the helix-coil transition, which are relevant to our investigations. In the first part, no constraints on the end-to-end distance R are assumed, whereas the second part investigates the effect of an externally imposed end-to-end distance R.

2.1 Unconstrained end-to-end distance

There are three main consequences if the polymer (or part of it) is found in a helical state: as the strand winds tightly around a central axis, the effective polymer length is shortened dramatically by a factor γ, which is about 0.4 for a typical polypeptide. Secondly, the hydrogen bonds prevent the monomers from free rotation, hence increase the effective persistence length from about $a_\mathrm{c} = 1.8$ nm in the coil state to $a_\mathrm{h} = 200$ nm in the helical state [7,6]. Thirdly, as the number of available configurations has decreased, the gain Δh in potential energy per monomer by forming hydrogen bonds competes with the associated loss of entropy Δs. The net balance is established by writing down the free energy per monomer:

$$\Delta f = \Delta h - T\Delta s, \tag{1}$$

where T is the temperature. Since Δh and Δs are both negative on formation of hydrogen bonds, we observe that at low temperature the formation of helices is promoted, whereas at high temperatures the coil state is favoured. Later, we shall have to distinguish two cases according to the sign of the net free energy difference Δf.

At this stage, the model is far from being exhaustive: monomers located at the ends of helical domains suffer a great entropy reduction, but do not form hydrogen bonds. Therefore each interfacial monomer between a coil and helical domain has an increased free energy of

$$\Delta f_t = -\Delta h, \tag{2}$$

compared to a monomer in the helical state. This additional interfacial energy contribution will suppress domain boundaries, and hence render the helix-coil transition in this model more cooperative.

In the literature, one normally gives the above model parameters Δf and Δf_t in terms of the Zimm-Bragg parameters s and σ [5], which are merely the exponentials of these quantities:

$$\begin{aligned} s &= \exp(-\beta\Delta f)\,, \\ \sigma &= \exp(-2\beta\Delta f_t), \end{aligned} \tag{3}$$

where $\beta = 1/(k_{\rm B}T)$ with $k_{\rm B}$ the Boltzmann constant. The factor 2 in equation (3) takes into account the fact that a helical domain has two interfaces with the coil domains, hence two monomers suffer from loss of configurational states, while they do not gain any additional energy from hydrogen bonds.

After identifying the microscopic states of the chain monomers $\{s_1 s_2 \dots s_N\}$, with $s_i = c$ or h for the monomer i to be in a coil or helical state, respectively, and their corresponding energetic contributions (see previous paragraph), relevant quantities of interest, *e.g.* the average helical fraction of an ensemble of polymers $\langle\chi\rangle$, can be determined by the usual statistical-mechanical calculation involving the partition function

$$Z = \sum_{\{s_1 s_2 \dots s_N\}} e^{-\beta F(\{s_1 s_2 \dots s_N\})}, \tag{4}$$

where the sum is performed over all possible states of the variables s_i, $i = 1, \dots, N$. The total free energy F, depending on the states $\{s_i\}$, is the sum of monomer free energy contributions (1) and (2). This procedure will also take a mixing entropy into account: for a fixed number of coil and helical domains, the sequence can be changed without energy change, provided that a helical domain follows a coil domain and vice versa. Therefore, configurations of shorter domain structure receive a higher statistical weight.

Experimentally, the average helical fraction in a solution of free polymers is accessible by measuring the net optical rotation of polarised light. However, experiments [10–12] deal with polymers in solution in different environmental conditions: a change in temperature or in another variable (pH value, salt concentration) affects the free energies Δf and Δf_t, hence by means of averaging over states, the average helical fraction χ is altered. Qualitatively, one can observe that at low temperature the optical rotation increases. Hence, one can conclude that the segments condense into helical domains, whilst at high temperature thermal fluctuations destroy the order and drive the segments preferably into the coil state.

Buhot and Halperin [13] pursue the evaluation of the partition function (4) with great care and demonstrate that a method merely based on a coarse-grained free energy approach leads to the same result as the transfer matrix method, the original treatment used by Zimm and Bragg [5], also used, for example, in [6,15].

In a first approximation, however, one can neglect the mixing entropy and follow a very simple route. We assume in the following that the helical and coil domains are artificially separated into just two blocks (cf. Fig. 2). This is equivalent to neglecting any form of cooperativity in the system: firstly, the entropy arising from reordering the domains (maintaining the alternating succession of coil and helical domains) is neglected, and secondly the interfacial energy is similarly disregarded.

The detailed investigation by Buhot and Halperin [13] showed that this simplification does not change the outcome qualitatively and only mildly quantitatively. Encouraged by their results, we apply a similar strategy here and treat the strands in a diblock approximation. Since we now neglect the effect of reordering the domains on the statistical weight, the system is microscopically described by the fraction of helical segments χ ($0 \le \chi \le 1$).

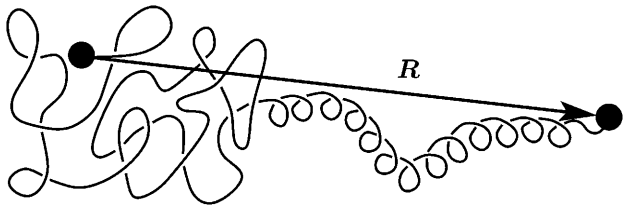

Fig. 2. An illustration of the diblock approximation: neglecting the entropy arising from the reordering of short helical segments is equivalent to assuming that helical and coil domains are separated into two coherent domains.

2.2 Fixed end-to-end distance

So far, the end-to-end distance R has been unconstrained. If, however, the chain has to span an externally imposed distance R between its ends, the system can only access a subset of configurations; in other words, it will suffer a reduction of entropy. This argument applies both to the coil and helical part of the chain. However, the cost of reducing the entropy is much higher for the coil part than for the helical part, since most of the configurational entropy in the helical part has been reduced anyway by the tight interlocking (bonding) between adjacent segments. Therefore, the helical segments become aligned between the externally fixed endpoints and the coil segments are tautened over the distance which cannot be bridged by the helical segment.

The free energy of the whole chain, under these assumptions, reads as follows:

$$F_{\rm ch} = \chi N \Delta f + 2\Delta f_t + F_{\rm coil}, \tag{5}$$

where N is the total number of monomers of length a. The free energy term $F_{\rm coil}$ describes a coil polymer with end-to-end distance R minus the amount of distance which can be bridged by the helical part.

To describe this last term $F_{\rm coil}$, we use the Gaussian approximation of an ideal random walk. This approximation breaks down at high extensions, but the practical quantitative deficiencies are not great as the investigations in reference [13] have revealed. We therefore have

$$\beta F_{\rm coil} = \frac{3}{2} \frac{1}{(1-\chi)Na^2} \left(R - \gamma a N \chi\right)^2, \tag{6}$$

taking into account the reduction in the contour length available for the coil and also the reduction of the effective coil end-to-end distance.

Before moving on and introducing the basic techniques for a network theory, we reproduce the findings for this model. The minimisation condition $\partial F_{\rm ch}/\partial\chi = 0$ allows us to determine the equilibrium value $\chi = \chi(R)$. Subsequently, by substituting $\chi(R)$ back into equations (5)

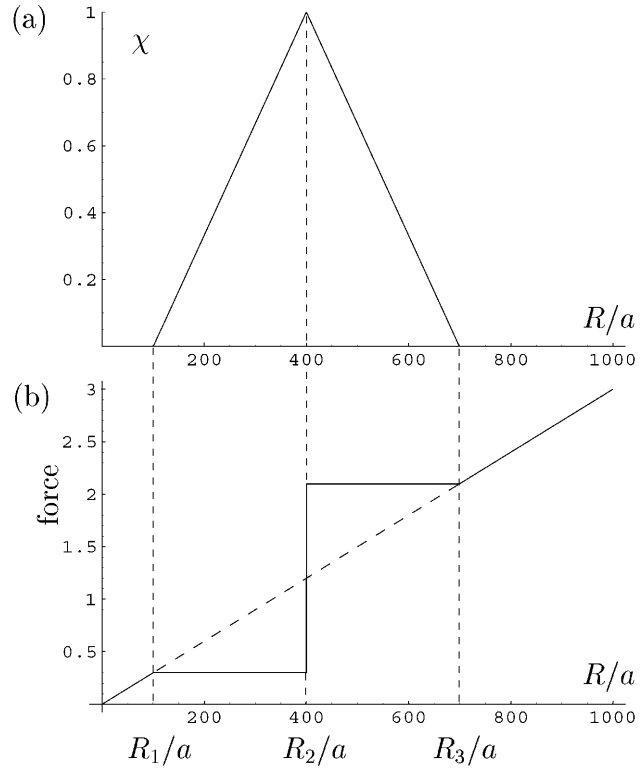

Fig. 3. This pair of diagrams shows the helical fraction χ (a) and the force (b), in units of $k_{\rm B}T/a$, *vs.* the end-to-end distance R. The parameters are as follows: number of monomers $N = 1000$, free energy of a helical state $\beta\Delta f = 0.1$, factor of shortening $\gamma = 0.4$. The dashed line shows the purely Gaussian behaviour of a free random walk. According to equations (7), $R_1 = 94.5a$, $R_2 = 400a$ and $R_3 = 705.5a$.

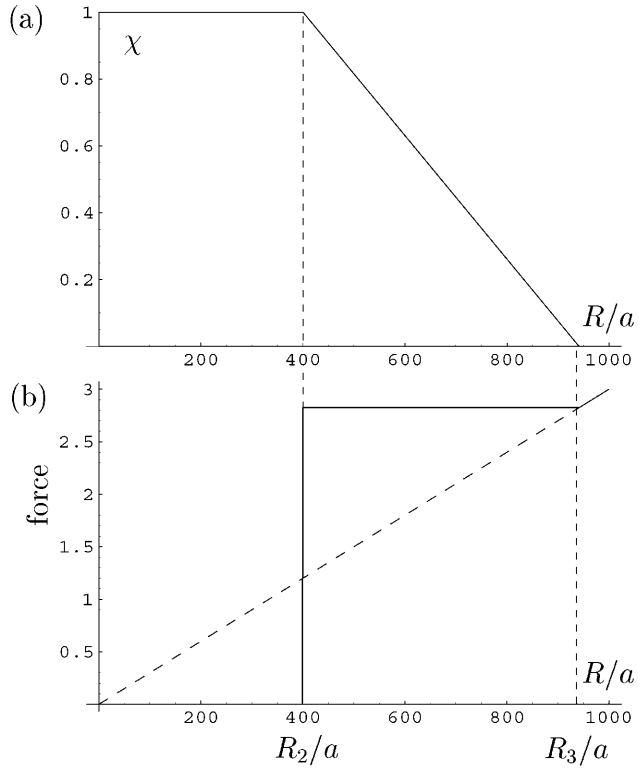

Fig. 4. The analogous plot as in Figure 3, but with an attractive interaction between helical monomers, meaning a negative free energy: $\beta\Delta f = -0.2$. All other parameters are the same as in Figure 3. Again, the dashed line indicates simple Gaussian behaviour of a model random walk.

and (6), we can obtain the effective free energy $F_{\rm ch}(R)$. At this point, we have to distinguish several cases.

We first look at the case $\Delta f > 0$. In the relaxed state at $R = 0$, there is no spontaneous formation of helical segments, simply because it would require a positive free energy $\Delta f > 0$ per segment to create a helix.

By pulling the endpoints apart, *i.e.*, by increasing R, one reduces the entropy of the coil, hence raises the free energy of the whole system. At a certain extension R_1, the increase in the free energy due to stretching matches the free energy required to transfer a monomer into a helical state. If the extension R is increased beyond R_1, then the molecule starts to form helical domains, at a constant force (see Fig. 3).

However, if the penalty for forming helical segments Δf is high, above a certain critical value $\Delta f_{\rm crit}$ (to be given below), this effect does not occur and the molecule stays in a coil state permanently, irrespective of the imposed stretching.

We are left to consider the case $\Delta f < 0$. At the statistically optimal $R = 0$, the molecule goes spontaneously into the helical state, driven by the net free energy gain. The end-to-end distance R can be increased without a big energy cost by aligning the helical segments. However, at an extension of $R_2 = \gamma aN$, the tight helical segments are torn apart and some stretched coil domains are created.

It is best to summarise the results in diagrams (Figs. 3 and 4), supplemented by analytical expressions. We show in two pairs of two diagrams the helical fraction χ *vs.* end-to-end distance R and the force extension curve, obtained from $\partial F_{\rm ch}/\partial R$.

It is useful to define the following auxiliary quantities:

$$\Delta R = a\gamma N\sqrt{1-\frac{\Delta f}{\Delta f_{\rm crit}}}\,, \qquad \Delta f_{\rm crit} = \frac{3}{2}\gamma^2 k_{\rm B}T\,.$$

We then can determine the three regime boundaries in the extension coordinate R:

$$R_1 = R_2 - \Delta R\,, \quad R_2 = \gamma aN\,, \quad R_3 = R_2 + \Delta R\,. \quad (7)$$

The function $\chi = \chi(R)$ is defined in the obvious way (see Figs. 3 and 4). For the force in response to the imposed extension R, one obtains the following expressions for the two cases, *i.e.* for the repulsive ($\Delta f > 0$) and

attractive ($\Delta f < 0$) case, respectively:

$$\text{force}|_{\Delta f>0} = k_{\mathrm{B}}T \begin{cases} \frac{3}{Na^2}R & \text{for } 0 \le R < R_1\,, \\ \frac{3}{Na^2}R_1 & \text{for } R_1 \le R < R_2\,, \\ \frac{3}{Na^2}R_3 & \text{for } R_2 \le R < R_3\,, \\ \frac{3}{Na^2}R & \text{for } R \ge R_3\,; \end{cases}$$

$$\text{force}|_{\Delta f<0} = k_{\mathrm{B}}T \begin{cases} 0 & \text{for } 0 \le R < R_2\,, \\ \frac{3}{Na^2}R_3 & \text{for } R_2 \le R < R_3\,, \\ \frac{3}{Na^2}R & \text{for } R \ge R_3\,. \end{cases}$$

From these equations for the force, one obtains expressions for the free energy $F(R)$ by integrating over R. These expressions involve, besides some constants, linear and quadratic terms in R.

The model is based on the Gaussian approximation, used to describe the random walk part of the chain. It assumes that the end-to-end distance of the coil part is much shorter than the coil's contour length. Therefore, the approximation breaks down at high extensions: the true force diverges [16]; however, the force derived using the Gaussian model remains finite (see Figs. 3 and 4). This artefact of the simplified model will later be compensated by the fact that, nevertheless, the Gaussian model correctly predicts a very low probability of finding a chain at such large extensions. To illustrate this effect, we refer to Figures 3 and 8 below: the abrupt surge in the force at R_2 implies that the free energy $F(R)$ increases at a much higher rate for $R \ge R_2$, hence the probability of finding a polymer with $R \ge R_2$ decays very rapidly. A more realistic model with a divergent force and free energy would only increase this effect.

3 Network theory

The fact that the polymer chains cannot intersect each other, implies that topological constraints and entanglements play a crucial role and alter the statistics significantly. However, a very simple theory can reproduce many basic experimental findings: the phantom chain network approach [16].

This model assumes that the polymer strands actually do not interact along their backbones, but only at their endpoints where they are linked to each other. Hence, the strands are effectively transparent to each other and are allowed to fluctuate freely, with only the end-to-end distance R constrained. This assumption is not as naive as it might appear: there are deep physical reasons why one can neglect self-interactions in a dense polymer system, and why lateral (tube-like) constraints do not matter until a topological knot is tied around the chain [16,17].

Within the Gaussian model of a random walk, the probability distribution of the end-to-end distance reads as usual [17]:

$$P(\boldsymbol{R}) \propto \exp\left(-\frac{3}{2Na^2}\boldsymbol{R}^2\right), \tag{8}$$

assuming that $|\boldsymbol{R}| \ll aN$, the chain contour length.

Accordingly, the free energy of a chain is quadratic in $\boldsymbol{R}$ for small extensions:

$$\beta F = -\ln P(\boldsymbol{R}) = \frac{3}{2Na^2}\boldsymbol{R}^2, \tag{9}$$

which implies a simple Hookian behaviour in response to stretching.

The distinctive feature of a network consists in memorising the initial end-to-end distance distribution of chains as they are crosslinked at their endpoints. In a simple network theory, one assumes that the polymers obey the equilibrium melt statistics when they are crosslinked. Hence, the statistical distribution of crosslinked network spans $\boldsymbol{R}$ obeys the Gaussian form (8). Since it turns out that for the overwhelming number of chains the condition $|\boldsymbol{R}| \ll aN$ is satisfied, the quadratic form for the free energy per chain (9) is well justified and can be used in the network calculation. This leads immediately to the average total free energy per chain in a random network:

$$F = \int \mathrm{d}\boldsymbol{R}\; F(\boldsymbol{R})\; P(\boldsymbol{R}). \tag{10}$$

Any external manipulation only affects the term $F(\boldsymbol{R})$ in equation (10), whereas the distribution $P(\boldsymbol{R})$ is left unchanged, it is said to be topologically quenched. For example, an affine macroscopic deformation $\underline{\underline{\boldsymbol{\lambda}}}$ of the whole body, which can serve as a good representation of the microscopic affine deformation of the network strands $\boldsymbol{R}$, only enters in the free energy, but leaves the distribution $P(\boldsymbol{R})$ unchanged. The elastic energy therefore becomes

$$F_{\mathrm{elast}}\big(\underline{\underline{\boldsymbol{\lambda}}}\big) = \int \mathrm{d}\boldsymbol{R}\; F(\underline{\underline{\boldsymbol{\lambda}}}\boldsymbol{R})\; P(\boldsymbol{R}),$$
$$\text{with } P(\boldsymbol{R}) \equiv \frac{e^{-\beta F(\boldsymbol{R})}}{\int \mathrm{d}\boldsymbol{R}\; e^{-\beta F(\boldsymbol{R})}}. \tag{11}$$

In general, the free energy $F(\boldsymbol{R})$ does not need to be quadratic (9), leading to non-Gaussian distribution $P(\boldsymbol{R})$.

An analogous reasoning will lead to the average helical content $\langle\chi\rangle$ of a network, which gives the total fraction of monomers in a helical state. Under the assumption that the end-to-end distance distribution at crosslinking obeys the equilibrium distribution $P(\boldsymbol{R})$ and is conserved in the crosslinked network, an imposed deformation $\underline{\underline{\boldsymbol{\lambda}}}$ leaves the distribution $P(\boldsymbol{R})$ unaffected, but does enter $\chi(|\boldsymbol{R}|)$. Thus, the dependence of the helical content χ on the deformation $\underline{\underline{\boldsymbol{\lambda}}}$ reads:

$$\langle\chi\rangle\big(\underline{\underline{\boldsymbol{\lambda}}}\big) = \int \mathrm{d}\boldsymbol{R}\; \chi\big(\big|\underline{\underline{\boldsymbol{\lambda}}}\boldsymbol{R}\big|\big)\; P(\boldsymbol{R}). \tag{12}$$

4 Network of helix-forming polymers

We now combine the theory for single molecules with the quenched averaging to calculate network properties. We will mainly focus on the total helical content described by equation (12). Since the helical fraction χ depends on

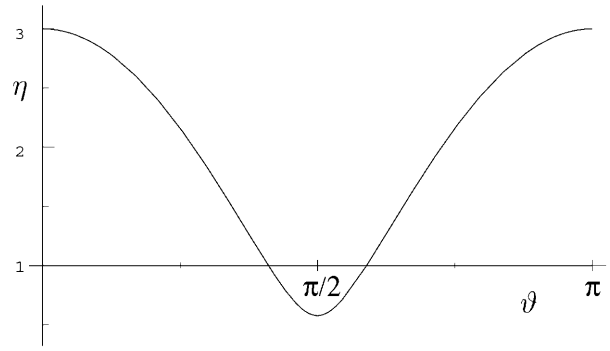

Fig. 5. The elongation and compression η of chains depends on the polar angle ϑ (cf. Eq. (14)). The scaling factor η becomes unity if $\arctan\vartheta = \sqrt{\lambda(\lambda+1)}$. Here, we have chosen $\lambda = 3$.

the end-to-end distance $\boldsymbol{R}$, we can expect that in a network, the average helical content $\langle\chi\rangle$ would depend on the deformation $\underline{\underline{\boldsymbol{\lambda}}}$, giving an opto-mechanical coupling.

To evaluate the integral in equation (12), note that all the functions, *i.e.* $F(R)$ and $\chi(R)$ uniquely depend on R, but are only analytically defined piecewise (*e.g.* see Eq. (A.1)) between the limits $R = 0$, R_1, R_2, R_3 and Na (see App. A). On the other hand, any incompressible deformation $\underline{\underline{\boldsymbol{\lambda}}}$, which we assume here, acts differently on different strands: some strands are expanded, whereas others are compressed, depending on the direction of the end-to-end vector $\boldsymbol{R}$ of a given strand.

We simplify the problem further by looking at uniaxial deformations along the z-axis only:

$$\underline{\underline{\boldsymbol{\lambda}}} = \begin{pmatrix} 1/\sqrt{\lambda} & 0 & 0 \\ 0 & 1/\sqrt{\lambda} & 0 \\ 0 & 0 & \lambda \end{pmatrix}. \tag{13}$$

The end-to-end distance of a strand which is initially aligned at an angle ϑ with the z-axis is therefore scaled by the factor η:

$$R' = \left|\underline{\underline{\boldsymbol{\lambda}}}\boldsymbol{R}\right| = \eta R\,,$$
$$\text{with} \quad \eta(\lambda,\vartheta) = \sqrt{\lambda^2\cos^2\vartheta + \frac{1}{\lambda}\sin^2\vartheta}. \tag{14}$$

As a result, the uniaxial deformation, as in equation (13), affects the end-to-end distance R differently according to the angle ϑ between the initial end-to-end distance $\boldsymbol{R}$ and the z-axis of the imposed deformation. For example, if $\lambda > 1$, this is tantamount to an extension by a factor λ along the axis of deformation ($\vartheta = 0$) and to compression by $1/\sqrt{\lambda}$ perpendicular to the axis ($\vartheta = \pi/2$), see Figure 5.

Clearly, one can see in Figure 5 that at two polar angles, for which $\tan\vartheta = \sqrt{\lambda(\lambda+1)}$, the end-to-end distance of the chains is not affected by the deformation. In other words, the set of vectors $\boldsymbol{R}$ invariant under the deformation $\underline{\underline{\boldsymbol{\lambda}}}$ lies on a cone, see Figure 6.

The boundaries between which the function $\chi\big(\left|\underline{\underline{\boldsymbol{\lambda}}}\boldsymbol{R}\right|\big) = \chi(\eta R)$ is analytically defined, are similarly scaled to R_1/η, R_2/η, or R_3/η, respectively. For

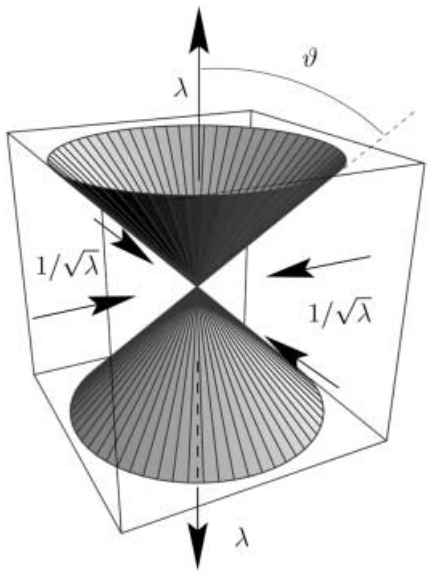

Fig. 6. The locus of strands which are invariant under the uniaxial deformation $\underline{\underline{\boldsymbol{\lambda}}}$ (13). The cone has an opening angle of $\vartheta = \arctan\sqrt{\lambda(\lambda+1)}$. For $\lambda > 0$, the arrows indicate the approximate deformation of chains.

a specific value η, one has to break up the radial R-integration in

$$\langle\chi\rangle(\lambda) = \int \mathrm{d}\Omega \underbrace{\int}_{\text{[piecewise]}} \mathrm{d}R\; R^2\; \chi(\eta R)\; P(R) \equiv \int \mathrm{d}\Omega\; I(\eta)\,, \tag{15}$$

not only at the values $R = R_1$, R_2 and R_3, but also at the values $R = R_1/\eta$, R_2/η and R_3/η.

Depending on the value of η, the breakup values adopt a particular order among themselves. At critical values

$$\eta_1 = \frac{R_3}{R_2} \quad \eta_2 = \frac{R_2}{R_1} \quad \eta_3 = \frac{R_3}{R_1}$$

some limits coincide, and as η crosses these values, the order of breakup limits is changed. We refer to the Appendix A for an explicit determination of regimes.

For any particular value of η, the R-integration can be carried out giving analytical expressions in η involving error functions. But for varying η, the integration regimes change, hence also the integrals. Therefore, the function $I(\eta)$ selects among a set of functions $I_i^{\pm}(\eta)$, depending on the value of η (see App. B),

$$\langle\chi\rangle(\lambda) = \int \mathrm{d}\varphi \int \mathrm{d}\vartheta\; \sin(\vartheta)\; I_{\text{select}}(\eta(\lambda,\vartheta)),$$

where $I_{\text{select}}(\eta)$ selects the appropriate expression for $I_i^{\pm}(\eta)$ depending on the value of η.

In the last step, the integration over the two angles φ and ϑ is carried out: the system is rotationally invariant, hence the integration over the azimuthal angle φ is trivial. The integration over the polar angle ϑ is carried out numerically.

5 Results and discussion

We demonstrate the effect of network averaging by going through a particular example. We choose the following parameters: $N = 1000$ and $\gamma = 0.4$, and first examine the case of $\beta\Delta f = 0.1$, that is when helix formation is unfavourable in equilibrium. Note that, for convenience, we give all quantities in dimensionless units, expressing lengths in units of the basic persistence length a.

On the one hand, the helical fraction χ of a single molecule with these parameters is peaked around $R_2 = 400a$ and the flanks end at $R_1 = 94.5a$ and $R_3 = 705.5a$ (see Fig. 3). On the other hand, the probability density distribution

$$P(R) = R^2 \exp(-\beta F(R)), \tag{16}$$

which is valid for the single molecule statistics and also for the network calculation, is peaked at a value $R^* = 30.8a$ (see Fig. 7). Therefore, the network average $\langle\chi\rangle$ for the undistorted network ($\lambda = 1$) will yield a very low helical content, as there are only very few chains present where $\chi(R) \neq 0$.

However, if a uniaxial extension, parametrised by λ (see Eq. (13)) is applied, then some chains are stretched and some are compressed (Fig. 6). As we have seen from equation (16), most of the chains are clustered near the shell of radius R^*. In pictorial terms, the uniaxial deformation now takes chains which are both near this shell and close to the axis of the deformation (*i.e.* around the poles of the R^* shell) to a deformed state: the chains will be clustered around two points on the axis at a distance λR^* from the origin. As the parameter λ becomes sufficiently large, the uniaxial deformation takes some increasing population of chains into a region where the helical fraction $\chi(\underline{\underline{\boldsymbol{\lambda}}}\boldsymbol{R})$ becomes non-zero.

Taking this reasoning to an extreme, we can think of large values for λ, where actually the chains are stretched to such a degree that they are transferred beyond the peak of $\chi(R)$ (cf. Fig. 7), that is, $\lambda R^* \geq R_2 \equiv \gamma a N$.

Moreover, the end-to-end distance of chains with $\boldsymbol{R}$ perpendicular to the axis is scaled by the factor $1/\sqrt{\lambda}$. Hence, for $\lambda > 1$, these chains are shrunken and thus, in our example, taken to a region where the helical fraction $\chi(R)$ is still zero.

On the other hand, if we consider a deformation with $\lambda < 1$, *i.e.* a compression along the z-axis with a simultaneous elongation in the plane perpendicular to the z-axis, then the roles are interchanged: for an appropriate λ, chains with $\boldsymbol{R}$ approximately of length R^* perpendicular to the axis are deformed to such a degree that the helical content $\chi(\underline{\underline{\boldsymbol{\lambda}}}\boldsymbol{R})$ becomes non-zero, whilst chains with $\boldsymbol{R}$ approximately along the axis are taken to regions where $\chi(\underline{\underline{\boldsymbol{\lambda}}}\boldsymbol{R}) = 0$.

Therefore, in the example considered (Figs. 3 and 7), compression and elongation both lead to an increase in the helical content, the latter however only at very high compression rates, hardly achievable in practice. The averaged helical content of this example is plotted in Figure 9 (dotted line) below.

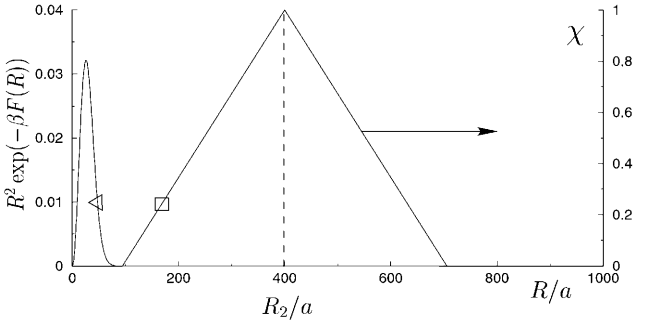

Fig. 7. The probability density equation (16), labelled by a triangle (left axis), and the helical fraction, labelled by a square (right axis). The former is peaked at about $R = 30.8a$, the latter at $R = \gamma a N = 400$, leading to a very low helical content in the network (see dotted line in Fig. 9). The parameters are those of Figure 3.

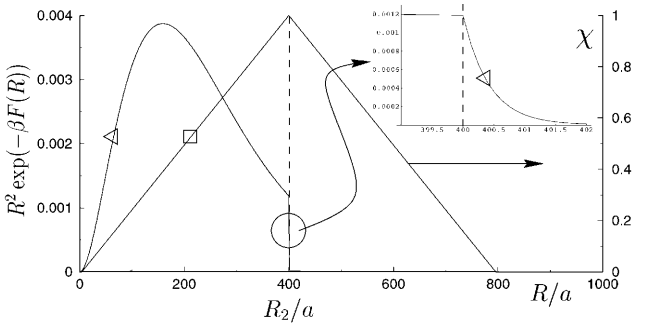

Fig. 8. The analogous plot to Figure 7, but now for much smaller $\beta\Delta f = 0.005$. There is a sufficiently high overlap of the probability distribution function and the helical fraction to generate a helical content in the network (see dashed line in Fig. 9). The inset shows the expanded region of the transition at R_2.

Another choice of parameter values gives a completely different behaviour. For an illustration of this, we refer the reader to Figure 8, which shows the behaviour of a chain with $\beta\Delta f = 0.005$, a much lower free energy penalty for the spontaneous helix formation. Now, the peak of the probability distribution is around $R^* = 159.2a$, whereas the helical fraction reaches the maximum at $R = 400a$. As these two functions now show a much larger overlap, the average helical content in a network is much bigger, and furthermore, it can be increased by both compression and elongation, see the dashed line in Figure 9.

Note that the probability distribution in Figure 8 justifies the Gaussian approximation used earlier in equation (6): for extensions above R_2, the free energy has an increased slope, therefore, the probability distribution shows a fast decay. In other words, chains at such high extensions correctly contribute very little to the quenched averaging, equations (11) and (12).

Figure 9 shows the different responses of the average helical content in a network for various positive values of the free energy $\beta\Delta f$. For negative values of the free energy, that is for polymers spontaneously folding into helices at

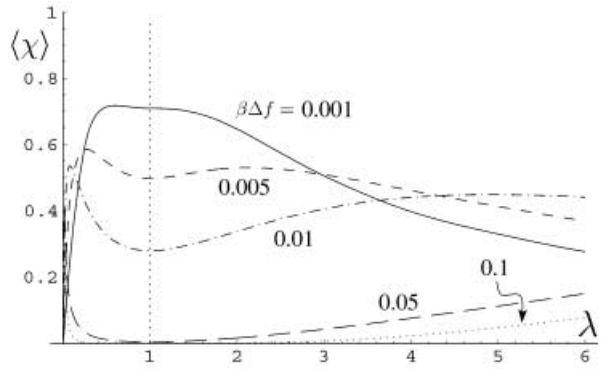

Fig. 9. The helical content in a network for different parameters. The free energy $\beta\Delta f$ takes the following values: 0.001 (solid line), 0.005 (dashed line), 0.01 (dot-dashed line), 0.05 (long-dashed line) and 0.1 (dotted line); the other parameters ($N = 1000$, $a = 1$) are kept constant.

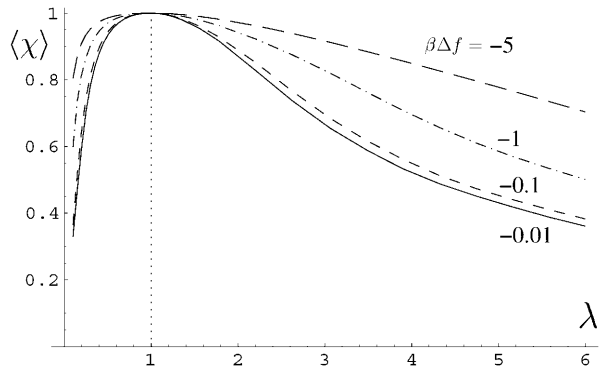

Fig. 10. The helical content in a network for different values of the free energy: $\beta\Delta f = -0.01$ (solid line), -0.1 (dashed line), -1 (dot-dashed line), and -5 (long-dashed line); the other parameters ($N = 1000$, $a = 1$) are kept constant.

given conditions, Figure 10 gives an analogous set of results. Note that in the limit $\beta\Delta f \to 0$, both cases converge to a qualitatively similar curve, although our model does not treat this case properly. In the limit of vanishing free energy penalty, the two cases give a different behaviour for the helical fraction of one single molecule. As $\beta\Delta f \to 0^+$, the helical fraction χ looks similar to Figure 3a, whereas for $\beta\Delta f \to 0^-$, χ resembles Figure 4a. This is the upshot of the fact that, in our model, there is a discontinuous jump in the helical fraction as Δf changes sign.

Moreover, the results inferred for the case of a negative free energy $\beta\Delta f$ have to be taken with some caution: the network theory, outlined in Section 3, assumes that the network consists of random coils, allowing one to use Gaussian statistics. However, for a negative free energy $\beta\Delta f$, the polymers spontaneously form helical, semiflexible chains, which will obey different statistics than flexible coil chains. Only for very long semiflexible chains, the Gaussian statistics are again recovered.

To summarise, we have calculated the average helical content in a network based on helicogenic polymer molecules described by a simple coarse-grained model. We found that a macroscopic deformation can have opposite effects on the helical content of the network: in the case of positive free energy $\beta\Delta f$, *i.e.* the formation of helical bonds leads to an overall increase of free energy (high-temperature regime), both an elongation and a compression can increase the overall helical content. The extent of this effect depends greatly on the parameters chosen for the polymer molecules. In the case where the formation of helical bonds is favoured by a free energy gain, the undeformed network exhibits a maximal helical content, and any deformation, either compression or elongation, decreases the helical content of the network.

We expect that these findings are relevant for investigations on biological polymer networks by optical measurement, for example gelatin. In this material however, the helices are formed by three strands which, on cooling, bind to each other to act as effective crosslinks. Therefore, our model cannot be applied straightforwardly. We have however demonstrated that microscopic effects of macroscopic deformation can be observed in a network.

S.K. enjoyed discussions with M. Rief and P. Nelson on this subject, and would like to acknowledge support from Corpus Christi College, Cambridge, from the Cavendish Laboratory, and from the Cambridge Overseas Trust.

Appendix A. Regimes

The integration domains of the R-integral in equation (15) are broken up in several regimes. Here we show how these regimes are determined and the integration carried out. We only investigate the R-integration, although we keep in mind that the factor η can assume a range of values, namely between λ and $1/\lambda$ (cf. Eq. (14)):

$$\langle\chi\rangle_R(\eta) = \int\limits_{\text{[piecewise]}} \mathrm{d}R\; R^2\; \chi(\eta R)\; e^{-\beta F(R)}\,.$$

Note that the dependence on λ and ϑ is hidden inside in the variable η.

The comprehensive enumeration of all possible integrals is very lengthy, thus we illustrate the general process by focusing on a particular example: we choose the repulsive case ($\beta\Delta f > 0$) in the second η-regime with $\eta_1 < \eta < \eta_2$ (see Fig. 3).

The functions $\chi(\eta R)$ and $e^{-\beta F(R)}$ both can be expressed analytically only in piecewise regimes:

$$\chi(\eta R) = \begin{cases} 0 & \text{for } 0 \le R < R_1/\eta\,, \\ 1 + \frac{1}{\Delta R}(\eta R - R_2) & \text{for } R_1/\eta \le R < R_2/\eta\,, \\ 1 - \frac{1}{\Delta R}(\eta R - R_2) & \text{for } R_2/\eta \le R < R_3/\eta\,, \\ 0 & \text{for } R \ge R_3/\eta\,; \end{cases}$$

$$\beta F(R) = \begin{cases} \frac{3}{2Na^2}R^2 & \text{for } 0 \le R < R_1\,, \\ \frac{3}{2Na^2}R_1^2 + \frac{3R_1}{Na^2}(R - R_1) & \text{for } R_1 \le R < R_2\,, \\ \frac{3}{2Na^2}R_3^2 + \frac{3R_3}{Na^2}(R - R_3) & \text{for } R_2 \le R < R_3\,, \\ \frac{3}{2Na^2}R^2 & \text{for } R \ge R_3\,. \end{cases} \tag{A.1}$$

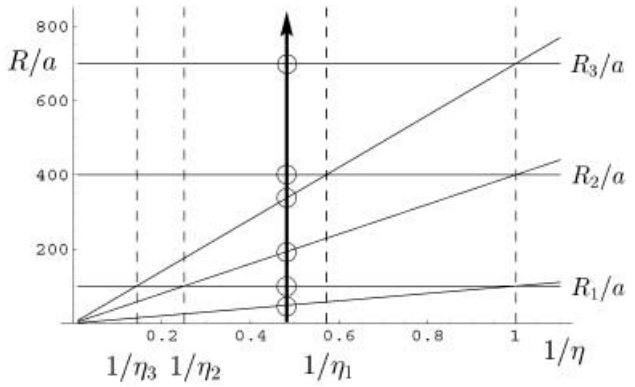

Fig. 11. The integration regimes, parameters as in Figure 3: number of monomers $N = 1000$ of length $a = 1$, net free energy difference for a monomer to be in a helical state $\beta\Delta f = 0.1$, factor of shortening $\gamma = 0.4$. These parameters imply: $1/\eta_1 = 0.57$, $1/\eta_2 = 0.25$ and $1/\eta_3 = 0.14$.

Appendix B. Integrals

The restrictions on the right-hand side of the equations (A.1) give the integration limits of the piecewise integrations. For our particular choice of η ($\eta_1 < \eta < \eta_2$), the integration path can be most easily determined by looking at Figure 11, where a typical integration path is highlighted together with the limits.

In this way, we are able to determine the appropriate limits of the integrals, *e.g.*:

$$
\begin{aligned}
I_{21}^{+}(\eta) &= \int_{0}^{\frac{R_1}{\eta}} \mathrm{d}R\; R^2\; \chi(\eta R)\; \exp(-\beta F(R))\,, \\
I_{22}^{+}(\eta) &= \int_{\frac{R_1}{\eta}}^{R_1} \mathrm{d}R\; R^2\; \chi(\eta R)\; \exp(-\beta F(R))\,, \\
&\vdots \\
I_{27}^{+}(\eta) &= \int_{R_3}^{\infty} \mathrm{d}R\; R^2\; \chi(\eta R)\; \exp(-\beta F(R))\,. \qquad \text{(B.1)}
\end{aligned}
$$

We then put the piecewise integrations together again to obtain

$$I_2^{+}(\eta) = \sum_{i=1}^{7} I_{2i}^{+}(\eta). \qquad \text{(B.2)}$$

Note that in the case of a net repulsive interaction ($\beta\Delta f < 0$), $\chi(\eta R)$ is zero for values $R < R_1$ and $R > R_3$. Therefore, the integrals in equations (B.1) vanish in these regimes, and the sum in (B.2) reduces to three terms only.

For a different values of $\eta > 1$, the procedure is exactly the same, giving $I_1^{+}(\eta)$, $I_2^{+}(\eta)$, etc. and analogously for values $\eta < 1$, we obtain $I_2^{-}(\eta)$, etc.

References

1. S.B. Smith, L. Finzi, C. Bustamante, Science **258**, 1122 (1992).
2. M. Rief *et al.*, Science **275**, 1295 (1997).
3. F. Oesterhelt, M. Rief, H.E. Gaub, New J. Phys. **1**, 6.1 (1999).
4. M. Rief, H. Grubmuller, ChemPhysChem **3**, 255 (2002).
5. B.H. Zimm, J.K. Bragg, J. Chem. Phys. **11**, 526 (1959).
6. A.Y. Grosberg, A.R. Khokhlov, *Statistical Physics of Macromolecules* (AIP Press, New York, 1994).
7. D. Poland, H.A. Scheraga, *Theory of Helix-Coil Transitions in Biopolymers* (Academic Press, New York, 1970).
8. H.A. Saroff, J.E. Kiefer, Biopolymers **49**, 425 (1999).
9. V.A. Bloomfield, Am. J. Phys. **67**, 1212 (1999).
10. A. Teramoto, Prog. Polym. Sci. **26**, 667 (2001).
11. S. Yue, G.C. Berry, M.M. Green, Macromolecules **29**, 6175 (1996).
12. P. Doty, J.A. Bradbury, A.M. Holtzer, J. Am. Chem. Soc. **78**, 947 (1956).
13. A. Buhot, A. Halperin, Macromolecules **35**, 3238 (2002).
14. A. Buhot, A. Halperin, Phys. Rev. Lett. **84**, 2160 (2000).
15. M.N. Tamashiro, P. Pincus, Phys. Rev. E **63**, 021909 (2001).
16. L.R.G. Treloar, *The Physics of Rubber Elasticity* (Clarendon Press, Oxford, 1975).
17. M. Doi, S.F. Edwards, *Theory of Polymer Dynamics* (Clarendon Press, Oxford, 1986).